Effects of Residual Ni60 Spray Particles on Structured-Blue-Light Scanning Accuracy of Helical Gears

Md Rakibul Islam
Master's Student
School of Mechanical and Electrical Engineering, China University of Mining and Technology, Xuzhou, Jiangsu China

Jingbin Hao
Associate Professor
School of Mechanical and Electrical Engineering, China University of Mining and Technology, Xuzhou, Jiangsu China

Md Oliwor Rahman
Master's Student
School of Mechanical and Electrical Engineering, China University of Mining and Technology, Xuzhou, Jiangsu China

Residual unmelted alloy particles left after laser cladding severely interfere with structured blue-light scanning for helical gear remanufacturing, resulting in incomplete surface data and distorted geometric measurements in actual production. This study prepared 20CrMnTi helical gear specimens in three steps with varying particle coverage levels and conducted comparative scanning experiments. Real-time images were captured for real-time scanning to observe surface optical changes, while surface completeness, mesh retention, and surface curvature deviation were calculated to evaluate the scanning performance. Experimental results revealed that both scattered and clustered particles triggered scanning defects, and built-in software processing could not fully eliminate errors caused by heavy contamination. A combined pre-scanning solution that included air cleaning, exposure adjustment, and multi-angle scanning was proposed. After treatment, the overall scanning quality of heavily contaminated gears improved significantly. The measurement indicators returned to levels close to those of the clean samples. This study provides reliable technical support for the standardized 3D measurement of laser-cladded gears in industrial remanufacturing practice.

Keywords: *Helical gear; Laser cladding; Residual spray particle; Structured blue-light scanning; Surface completeness.*

1. INTRODUCTION

Helical cylindrical gears with twisted involute working surfaces are core load-bearing transmission components widely used in mining reducers, automobile gearboxes, and wind-power speed-increase devices. Long-period alternating contact fatigue easily triggers pitting corrosion, tooth flank abrasion, and root crack failure, directly leading to a complete transmission shutdown and high replacement costs. Compared with manufacturing new gears from blanks for failed parts, laser cladding directed energy deposition (DED) remanufacturing realizes local damaged surface repair via high-energy laser molten alloy powder deposition, cutting raw material consumption by 60%–75% and reducing comprehensive production expenses significantly. This method has been popularized in domestic and international remanufacturing industries since 2015. 20CrMnTi carburized steel is the most widely used substrate material for medium-load industrial helical gears because of its balanced surface hardness and core toughness, while Ni60 nickel-based self-fluxing alloy is the universal cladding powder for gear surface restoration owing to its outstanding wear and corrosion resistance after solidification [5,13,15,16].

Most studies on gear laser cladding scanning preprocessing uniformly adopt ultrasonic cleaning with high-pressure air blasting to thoroughly eliminate surface attachments before scanning, thereby establishing experimental conclusions on an ideal particle-free gear working surface without simulating the real workshop environment. During the actual Ni60 laser cladding feeding process, partial alloy powder fails to be fully molten inside the laser molten pool under fluctuating laser power and unstable carrier gas flow, forming 20–150 μm granular unmelted spray particles splashing and adhering randomly on the tooth flank and concave root fillet; the unique twisted helical surface geometric structure easily traps residual particles and blocks complete pre-scan cleaning. Such adhered micro-particles induce irregular, diffuse reflection and local overexposure during structured-light projection, generating numerous stray noise points, regional point-cloud missing-hollow areas, and distorted involute contours after model reconstruction, eventually causing incorrect cladding allowance calculations and failed repair forming [6,22,24,27,29,31].

A systematic literature review revealed that no peer-reviewed published paper synchronously recorded real-time in situ scanner field-of-view optical image to intuitively map particle distribution with scanning noise morphology, and lacked systematic quantitative quantification linking particle coverage ratio with five core gear geometric deviation indexes; relevant error formation optical mechanism and targeted pre-scanning optimization scheme based on real scanning view evidence are also vacant in current research field [1-9,13,15,16]. This prominent research gap impedes the

Received: June 2026, Accepted: July 2026
Correspondence to: Md Rakibul Islam, Faculty of Mechanical & Electrical Engineering, China University of Mining and Technology, Xuzhou, Jiangsu, China
E-mail: mdrakibulislam.bgd@gmail.com
doi: 10.5937/fme2603515I

formulation of a unified specification for scanning operations for post-cladding-contaminated helical gears in remanufacturing factories [21,32].

To address this issue, this study captures real-time in-situ scanning images of helical gear specimens under three particle contamination levels (clean, low, and high coverage) using the scanner's built-in camera, enabling visual comparison of structured-light reflection varia–tions induced by residual Ni60 spray particles. Quantify five key evaluation parameters (point-cloud noise proportion, surface data completeness, involute profile deviation Δfα, helix slope deviation Δfβ, and single-tooth thickness measurement error) for all experimental groups using professional point-cloud post-processing software. Clarify the optical disturbance mechanism of cladding spray particles in structured blue-light projection against a helical involute curved surface, combining real scanning views and measured numerical data. Propose operable, low-cost pre-scanning optimi–zation solutions targeting particle-induced scanning defects and verify error reduction effectiveness via supplementary verification scanning tests.

This study innovatively combines synchronous in-situ real scanner field-of-view screenshots to reveal the differentiated optical interference mechanism of Ni60 particles on twisted helical involute surfaces. Smooth 20CrMnTi steel generates stable specular reflection of 420 nm blue structured light, while rough granular attachments produce omnidirectional diffuse scattering. Real scanning visuals distinguish two defect modes: scattered particles only create recoverable discrete noise, whereas clustered particles form permanent unfillable shadow blind zones concentrated at concave tooth fillets, reasonably explaining why helical gears are more sensitive to particle pollution than spur gears. Mean–while, a unified visual-quantitative joint evaluation sys–tem integrating scanning texture images, raw point cloud meshes, and multidimensional geometric errors is constructed, forming a replicable experimental paradigm for metrology research on other additive-manufactured curved metal components, which enriches the basic theory of structured-light triangulation measurement.

All grouped real scanning previews, mesh compa–rison figures, and tabulated quantitative error data in the manuscript can be directly compiled into standardized pre-scanning operation manuals for automobile gear–boxes, mining reducers, and wind power speed-up box production lines. Front-line operators can rapidly judge surface contamination severity by comparing the visualized scanning defects summarized in this study, so as to select matching pretreatment processes and effectively reduce the reject rate of remanufactured helical gears induced by inaccurate reverse modeling. The experimental specimens adopted m = 2, z = 40, 20° helix angle, and 20CrMnTi helical gears and universal Ni60 cladding powder, which represent mainstream medium-load transmission gear configurations. The testing workflow and evaluation indicators have strong universality and can be extended to the measurement of spur gears, bevel gears, and gears of different modules, helping small and medium-sized remanufacturing enterprises without professional optical laboratories to establish internal quality control standards and lower technical barriers of high-precision reverse engineering.

From economic and industry standardization pers–pectives, the proposed pretreatment method avoids repeated secondary scanning and gear scrapping; for medium-scale remanufacturing factories with hundreds of gears processed monthly, it can cut alloy powder consumption and post-machining workload by approxi–mately 15–20%, greatly lowering comprehensive pro–duction costs. At present, there are no dedicated in–dustrial specifications regulating pre-scanning pretreat–ment and acceptable residual particle limits for laser-cladded gears. The gradient contamination test data and validated optimization process provided in this study offer systematic experimental support for the drafting of unified industry measurement standards, standardizing disordered on-site scanning operations, and improving the overall dimensional consistency of remanufactured transmission gears. The research results serve three core groups of industrial practitioners: front-line scanning operators for daily pre-inspection, enterprise quality engineers for formulating measurement acceptance criteria, and industry standardization researchers for compiling remanufacturing technical specifications.

2. EXPERIMENTAL METHODOLOGY

The test substrate adopts an industrial-standard 20CrMnTi carburized helical cylindrical gear with fixed nominal geometric parameters.

2.1 Helical Gear Specimen Preparation & Step Division

Three mutually independent experimental steps were designed to conduct controlled comparative tests under identical machining and cladding pretreatment condi–tions. The basic geometric dimensions of the tested helical gear are presented in Figure 1.

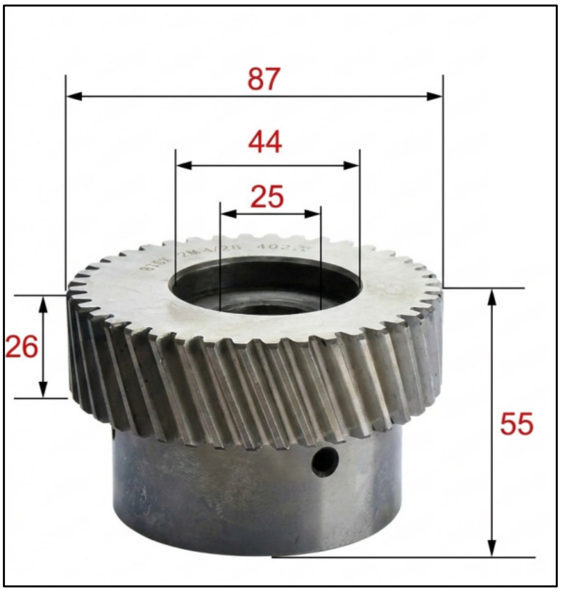

Figure 1. Basic Parameters of Helical Gear

Step 01: Clean the original helical gear thoroughly via ultrasonic cleaning and high-pressure dry air blowing, ensuring that no residual spray particles adhere to the entire tooth surface. The cleaning process is shown in Figure 2.

Step 02 (Medium particle coverage group): Artificially attach screened Ni60 unmelted cladding spray particles with a particle size of 20–60 μm. The particle coverage rate on the tooth working flank was controlled within 6%–11%. The particle application process is displayed in Figure 3.

Step 03 (High Particle Coverage Group): Mixed Ni60 particles ranging from 20 to 150 μm were applied, with the surface particle coverage rate maintained at 28%–37%, to simulate severe particle accumulation ca– used by inadequate on-site cleaning after laser cladding.

Table 1. Geometrical Parameters of the Experimental Helical Gear

Parameter	Geometrical		
	Symbol	Value	Unit
Gear type	–	L/H	–
Material	–	20CrMnTi	–
Module	m	2	mm
Number of teeth	z	40	–
Outside diameter	d_a	87	mm
Bore diameter	d_b	25	mm
Hub diameter	d_h	44	mm
Face width	b	26	mm
Overall height	H	55	mm
Pressure angle	α	20	°
Helix angle	β	~20	°

Figure 2. Maintenance Cleaning of Original Helical Gear

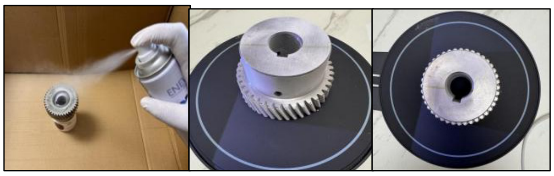

Figure 3. Application of 3D scanning spray on the helical gear

All test particles were collected from the real laser-cladding waste powder of Ni60 alloy used in an indus– trial gear remanufacturing production line to ensure that the particle chemical composition, surface morphology, and refractive index were consistent with those of actual residual spray particles after the cladding process [31].

The overall structure and working principle of the structured-blue-light 3D scanning system for gear inspection are illustrated in Figure 4.

As shown in Figure 4(a), the experimental platform comprised an EinScan SE V2 structured-blue-light sca– nner, a motorized rotary turntable, a 20CrMnTi helical gear specimen, and an industrial computer installed with EX–ScanS software. The scanner was fixed above the gear to maintain a stable working distance during data acquisition.

The main components, including the structured-blue-light projector, dual CMOS cameras, scanner mounting assembly, and rotary turntable fixture, are presented in Figure 4(b). During scanning, the gear rotated continuously on the turntable while the scanner projected blue structured light onto tooth surfaces. Reflected optical signals were captured by dual CMOS cameras and transmitted to the industrial computer via a USB 3.0 interface, as shown in Figure 4(c). The acquired images were further processed to generate 3D point clouds for geometric reconstruction and scanning quality evaluation. The constructed platform delivers a stable non-contact measurement setup for investigating how residual Ni60 spray particles affect the scanning accuracy of helical gears

2.2 Characteristics of Residual Ni60 Cladding Spray Particles

Incomplete melting during laser cladding produces irregular near-spherical and flaky residual particles with rough surfaces. These particles exhibited distinct light reflectivity compared to the smooth surface of the machined 20CrMnTi gear steel. Rough particles convert the specular reflection of structured blue light into diffuse scattered reflection, which is the primary cause of scanning data distortion [22,24]. The main elemental composition of the applied Ni60 self-fluxing alloy powder is listed in Table 2.

Table 2. Elemental composition of the Ni60 self-fluxing alloy powder

Constituent	Cr	B	Si	C
Percentage (wt.%)	15.8	3.2	4.1	0.75

The chemical composition of the 20CrMnTi helical gear substrate is given in Table 3.

Table 3. Chemical Composition of the 20CrMnTi Helical Gear Specimen

Constituent	C	Si	Mn	Cr	Ti	Fe
Percentage (%)	0.21	0.27	0.95	1.15	0.07	97.35

Standard mesh sieves are used for particle size screening. Fine particles (20–60 μm) are prepared for the S2 group, and mixed coarse particles (80–150 μm) are adopted for the S3 group.

2.2 Structured-Blue-Light 3D Scanning System & Real-Time Scanning View Capturing Setup

A commercial EinScan SE V2 portable structured blue-light scanner was used to acquire full-surface data of the tested helical gears.

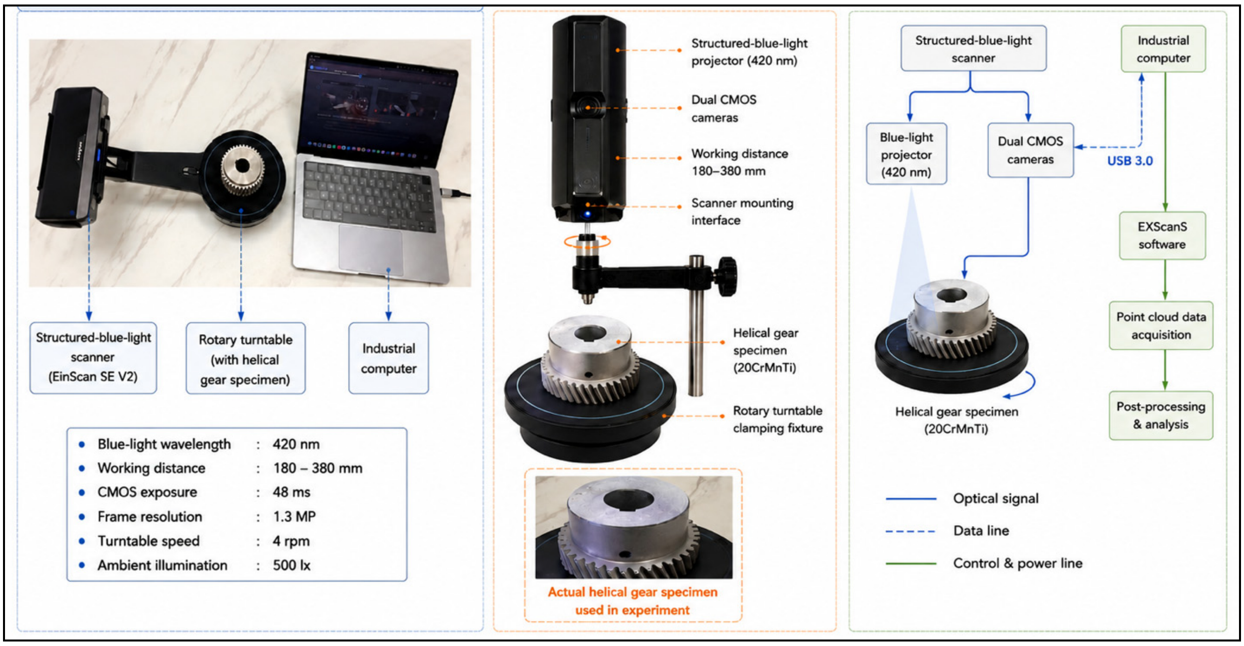

Figure 4. Experimental setup and working principle of structured-blue-light 3D scanning for helical gear inspection. a) Complete hardware system of structured-blue-light scanning for helical gears (b) Partial assembly diagram of scanning system (c) Working principle diagram

The scanner integrates dual high-resolution CMOS cameras to synchronously capture real-time in-situ preview images frame-by-frame during periodic blue fringe projection, with fixed experimental parameters maintained consistently across all three specimen groups: effective working distance ranging from 180 mm to 380 mm, central blue structured-light wavelength of 420 nm, single-frame image resolution fixed at 1.3 MP, baseline CMOS exposure value set at 48 ms, uniform rotary turntable rotational speed of 4 rpm, and stable indoor ambient illumination controlled at 500 lx throughout all scanning trials. All environmental vari–ables, including laboratory room temperature (25 ± 2 °C), surrounding stray light distribution, and gear clam–ping position relative to the scanner optical axis, were strictly controlled to eliminate extrinsic measurement deviations induced by fluctuating test conditions.

Two specialized software platforms were configured for subsequent post-processing and quantitative calcu–lation. Cloud Compare V2.13 was employed to perform raw point cloud filtering, stray-noise counting, and sta–tistical extraction of surface missing-area ratios. Geo–magic Design X 2024 was used for coordinate align–ment between scanned point cloud datasets and the no–minal CAD gear model, as well as for numerical fitting of involute profile deviation and helix slope error, following ISO 1328 standards [9,19]. During full-circumference automatic rotary scanning of every specimen, continuous real-time preview screenshots were automatically archived via the EXScanS native software interface; these stored in situ scanning images serve as fundamental visual evidence for subsequent correlation analysis between surface particle distribution and resultant scanning defects.

2.3 Defined Quantitative Scanning Error Evaluation Indicators

Following ISO 1328 gear specification and structured-light measurement criteria, five evaluation indicators were defined with the gear's nominal CAD model as the benchmark [26]. The selected metrics include the point cloud noise percentage, surface completeness, involute profile deviation $\Delta f\alpha$, helix slope deviation $\Delta f\beta$, and single-tooth thickness error. These indices quantify separately the proportion of stray noise, incomplete scanned area, and geometric deformation of the tooth profile induced by residual spray particles. Consistent post-processing parameters are applied to S1, S2, and S3 specimens to ensure reliable result comparison.

3. EXPERIMENTAL SET-UP AND PROCEDURE

The overall experimental testing system comprised an EinScan SE V2 portable blue structured light 3D scanner, precision rotary turntable, height-adjustable scanner support stand, and supporting industrial computer equipped with dedicated scanning and point-cloud processing software. The tested 20CrMnTi helical gear workpiece was rigidly mounted onto the central clamping fixture of the rotary turntable to avoid shifting or eccentric vibrations during circumferential scanning. The 3D scanner was fixed on an adjustable stand to maintain a constant operating distance from the gear tooth surface. Indoor room temperature and ambient illumination were strictly maintained consistently across all three specimen measurement batches, eliminating unpredictable environmental interference that may affect the structured-light projection and point-cloud acquisition accuracy.

Before initiating any specimen scanning operation, the system was calibrated using the original SHINI–NG3D calibration board marked CPCY 2203311676-V200. Following the software prompts, the calibration plate was placed at the designated turntable position and remained fixed throughout the calibration process until the software confirmed successful parameter matching. Afterwards, unified white-balance calibration is perfor–med under a fixed experimental ambient light to correct background light interference in structured-light fringe imaging, and the core original scanning parameters, including CMOS exposure value, single-frame resolution, and turntable rotation speed, are locked and remain unchanged for the S1 clean group, S2 low-particle group, and S3 high-particle group

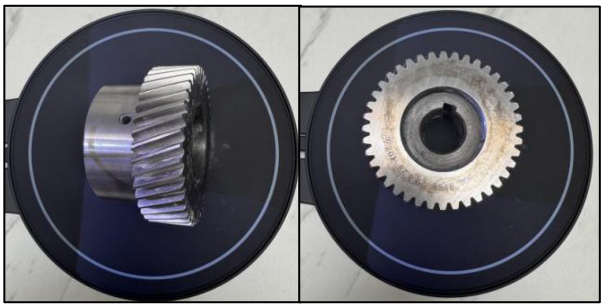

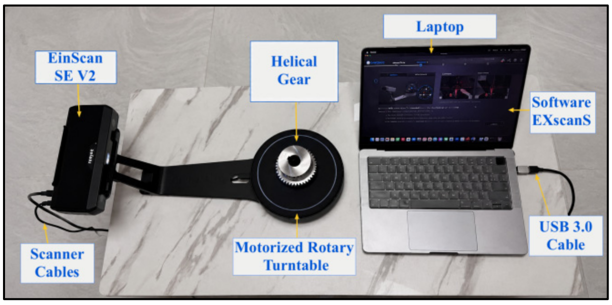

Figure 5. Experimental setup for 3d Scanning of Helical Gear

The EXscan SE V2 software shown in Figure 6c was activated to build an independent experimental project and input the standard geometric parameters of the tested helical gear in advance. Three differently pre-treated gear samples were sequentially installed on the turntable, with the installation posture carefully adjusted to ensure that the gear rotation axis coincided with the central axis of the turntable.

The formal data acquisition stage begins with auto–matic rotary scanning mode. As the turntable rotates at a uniform, predefined speed, the scanner continuously projects periodic blue structured-light fringes onto the involute tooth surfaces and root fillets in synchrony. The embedded high-resolution CMOS cameras inside the scanner record real-time in situ scanning views frame by frame, and all captured preview images are automatically saved to the designated system folder as intuitive original visual data. Once full-perimeter scanning for one gear specimen is accomplished, the complete raw point cloud dataset is stored and exported from the scanning software.

After completing baseline scanning for three groups, the exported point cloud data is imported into Cloud Compare V2.13 and Geomagic Design X 2024 separately to calculate the point cloud noise proportion, surface data completeness, and three types of gear geometric deviation indicators. Upon completion of the original group measurement, the high-particle-coverage S3 gear is processed using three proposed pre-scanning optimization approaches, and the same equipment calibration, clamping, and full-scanning procedure is then used in a supplementary verification test to collect optimized experimental data for comparative analysis.

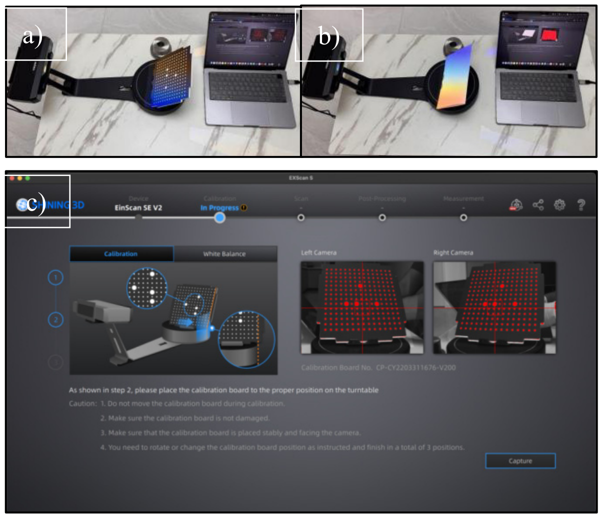

Figure 6. a) Caliberation of 3d Scanner. b) White Balance of 3d Scanner. c) EXscan SE V2 Software Interface

4. EXPERIMENTAL RESULTS & ANALYSIS

All real-time scanning previews presented in this sec–tion were captured directly from the native interface of the EXScanS scanning software, which intuitively recorded the full data acquisition and post-processing workflow for the three test groups: S1 clean gear without any adhered Ni60 spray particles, S2 medium spray-contaminated gear, and S3 high spray-conta–minated gear. The comparative analysis was divided into four sequential parts, corresponding to the raw tex–tured preview, raw non-textured preview, post-optimi–zation textured mesh, and post-optimization non-tex–tured mesh, as shown in Figure 7 to Figure 9, sys–tematically revealing the influence of residual cladding particles on the structured light scanning quality and the improvement effect of the built-in software mesh optimization algorithm.

4.1 Textured raw scanning preview

Figure 7 displays multi-angle, real-time, textured-scan–ning snapshots of the clean helical gear without residual spray particles captured dynamically during rotary auto–matic scanning before any mesh correction operation.

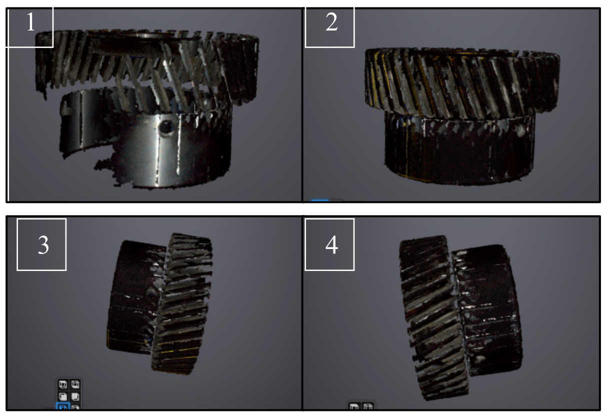

Figure 4-1: In-situ real-time scanning texture preview of clean helical gear specimens under different surface particle contamination levels

The six subgraphs record successive scanning pers–pectives along the turntable rotation path; the gear involute flank surface exhibits a continuous, uniform metallic texture without scattered abnormal highlight speckles or irregular blank shadow regions on the tooth root fillets. Benefiting from regular specular reflection of a smooth machined steel surface, the structured blue fringe projected by the scanner forms complete effective reflected signals; hence, the raw real-time preview achieves nearly full-surface data coverage with negligible local missing geometry, which sets an ideal baseline reference for subsequent contaminated specimen comparison.

Non-textured raw scanning preview

The corresponding non-textured raw point cloud preview of the same clean gear is shown in Figure 8, extracted directly from the raw mesh display module of the EXScanS software before mesh refinement. From the six diversified observation orientations, the preliminary blue raw mesh reproduces the complete helical gear outline and detailed involute tooth profile; only sporadic tiny isolated floating stray points emerge at individual tooth edges, and no large-area hollow missing holes are found on the tooth flank and root concave area. This raw non-textured result further verifies that a particle-free smooth gear surface can obtain a highly complete initial scanned point cloud under fixed scanning parameters.

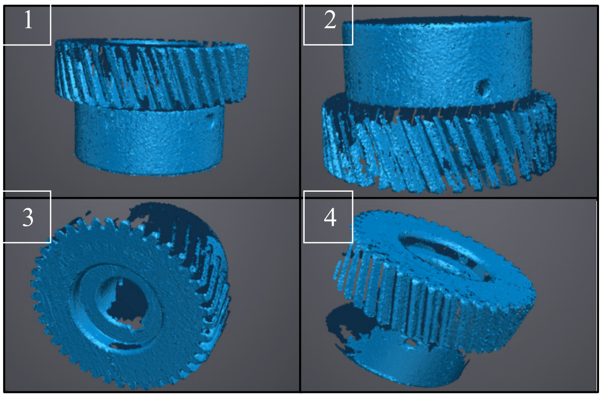

Figure 8. In-situ real-time scanning non-texture preview of clean helical gear specimens under different surface particle contamination levels

4.3 Post-optimization textured mesh preview

The upper layout of Figure 9 presents a multi-angle textured gear preview of a low-particle-contaminated sample after completing the full set of EXScanS mesh optimization procedures, including floating point removal, automatic hole filling, and surface smoothing. Compared with the raw textured preview of the clean gear, subtle irregular dark speckle traces retained on partial tooth surfaces correspond to diffuse reflection disturbances induced by medium-density adhered Ni60 spray particles [6,22]. After automatic software repair, most scanning blank voids caused by particle light scattering were filled, and the overall textured surface became continuous and intact, without obvious geometric fractures. Six arranged perspective views fully exhibit the complete outer contour of the optimized textured model for follow-up visual inspection.

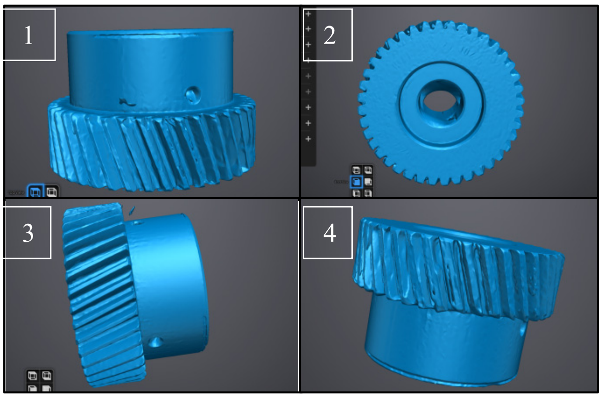

Figure 4-3: Mesh optimization preview of low particle helical gear scanned mesh in scanner post-processing module without texture.

4.4 Post-optimization non-textured mesh preview

The bottom panel of Figure 10 shows the final refined solid blue non-textured mesh derived from the same low-contamination specimen after a consistent postprocessing workflow. The surface bump distortion of the original raw mesh and scattered micro-gaps caused by low particle counts were substantially eliminated through algorithmic optimization. From six different rotary observation angles, the optimized non-textured mesh uniformly fits the standard helical gear geometric features, and the tooth involute profile and root fillet curve are restored to regular design morphology, thereby directly demonstrating that EXScanS native mesh optimization can effectively compensate for partial scanning defects originating from low-level particle contamination.

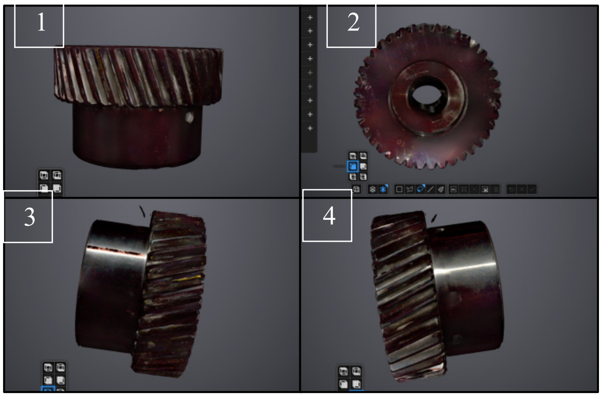

Figure 10. Mesh optimization preview of low particle helical gear scanned mesh in scanner post-processing module with texture.

Visual Comparative Analysis of In-Situ Scanning for Medium-Dose Spray Contaminated Gear

Real-time in situ scanning screenshots captured from the structured blue-light scanner interface are summarized in Figures 10 and 11 to visually characterize raw scanned surface features and subsequent mesh post-processing effects for the medium-particle-contaminated helical gear (S2 group) after artificial Ni60 spray particle deposition.

Figure 4-5 shows textured live-scanning previews and the corresponding optimized solid-mesh results for the medium-contaminated specimen.

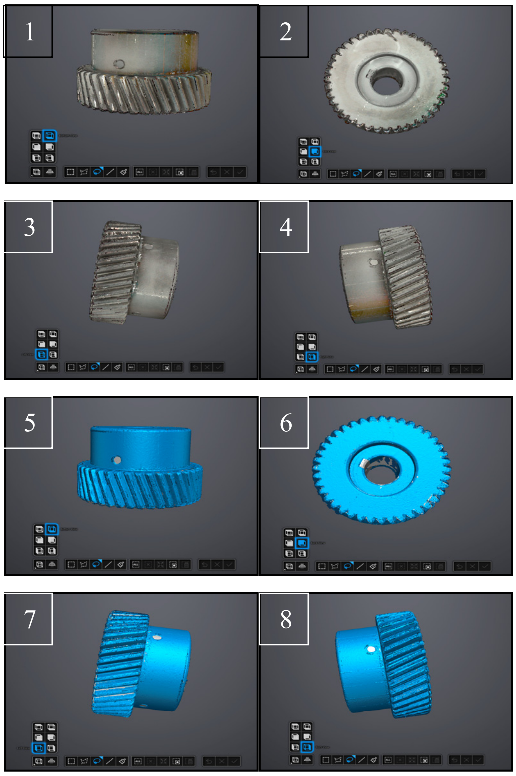

Figure 11. In-situ textured real-time scanning preview of medium spray-contaminated helical gear: upper row, raw textured multi-angle scanning snapshots captured during structured-light acquisition; lower row, preliminarily optimized solid mesh after primary scanner post-processing.

The upper four subplots show multi-angle raw tex–tured scanning views captured directly during on-mac–hine data acquisition; scattered, irregular bright speckles are distributed randomly over involute tooth surfaces and root fillets, originating from the omnidirectional diffuse reflection of incident blue structured light off rough, adhered Ni60 residual particles. These high–lighted speckle regions correspond to local stray point-cloud noise and sporadic missing-data blind zones quantified in the foregoing surface completeness calcu–lation. The bottom-row subplots display the homoge–nized solid-blue mesh derived from primary scanner post-processing, in which preliminary automatic hole-filling and noise suppression are applied to repair par–tial-scan voids caused by particle-induced optical disturbances.

Figure 12 further demonstrates a stepwise non-textured mesh optimization workflow in the scanner-dedicated post-processing module. Panels 1–4 present the original, unrefined raw meshes obtained from four distinct rotary scanning orientations; obvious surface irregularities, micro-protrusions, and intermittent surface gaps can be observed on the tooth flank and root geometry owing to uneven particle diffuse-reflection interference. Following sequential post-processing operations, including outlier vertex deletion, small floating-surface elimination, and automatic cavity filling, the optimized smooth, non-textured meshes (Panels 5–8) are generated for follow-up geometric error fitting and 3D model comparison.

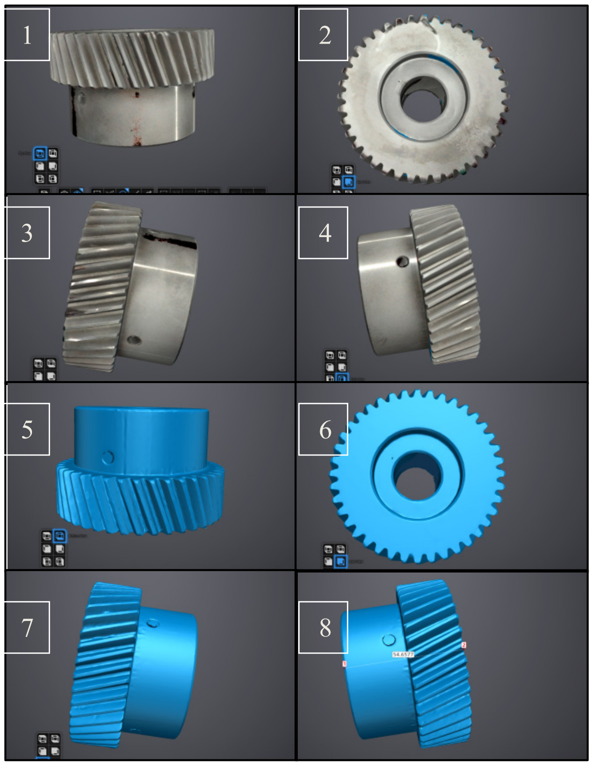

Figure 12. Stepwise non-textured mesh optimization pre–view of medium-contaminated gear within scanner post-processing module: panels 1–4, unprocessed raw mesh at different scanning perspectives; panels 5–8, finalized refi–ned non-textured mesh after built-in mesh repairing and smoothing treatment.

Visual Analysis of In-Situ Scanning Results for High-Concentration Spray-Contaminated Specimens

Figure 13 shows a multi-orientation-optimized, non-textured mesh of the high-particle-contaminated helical gear after EXScanS' built-in mesh post-processing. Compared with the low- and medium-contaminated counterparts, dense-accumulated Ni60 spray particles trigger severe, continuous, and diffuse reflection during structured-light scanning, generating large-area data loss concentrated at the gear inner bore, marked by a purple unfilled void in the rightmost subplot.

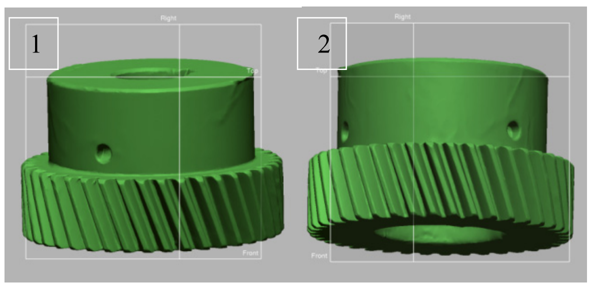

Figure 4-7. Multi-angle optimized non-textured solid mesh of high-concentration spray-contaminated helical gear

Although software optimization eliminates scattered surface noise and minor micro-gaps across the tooth flanks, the centralized massive blank region cannot be fully compensated by algorithmic hole-filling alone [29]. The optimized mesh exhibited visible surface unevenness on the cylindrical boss and root fillet, which originated from the interpolation smoothing applied to the extensive missing scanning data.

This visual result aligns with prior calculated surface completeness data for the S3 group, confirming that excessive high-density particle coverage leads to irreversible scanning defects that cannot be fully fixed by conventional scanner post-processing alone [25,32].

Quantitative Analysis of Point-Cloud Quality Index

Quantitative calculations of effective scanned area, sur–face completeness, mesh retention, and surface curva–ture deviation are performed for three specimen groups (S1: clean gear with zero particle adhesion; S2: low particle coverage gear; S3: high particle coverage gear). All consolidated computational results are summarized in Figure 12, which integrates three segmented data tables [(a) Surface completeness data; (b) Mesh vertex & face retention statistics; (c) Curvature deviation met–rics] and is positioned directly below the in-situ real scanning preview images (Figure 13).

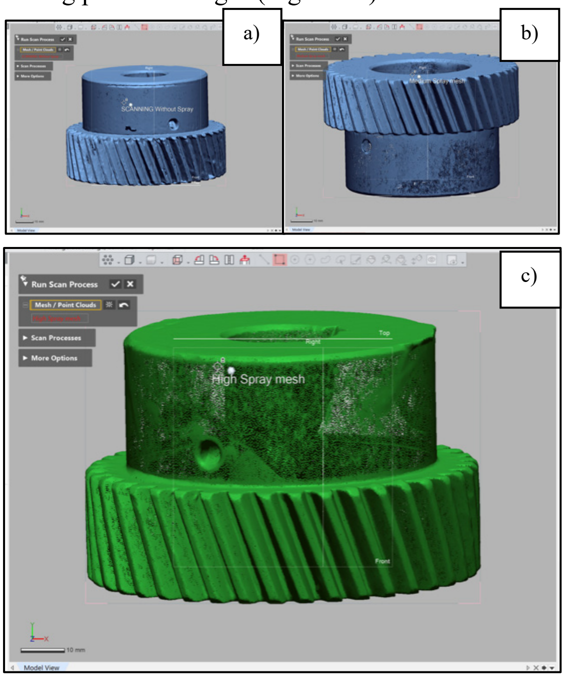

Figure 4-8. Non-textured scanned mesh morphology of helical gear specimens under different residual particle coverage levels: (a) clean gear without spray particles; (b) low particle coverage specimen; (c) high particle coverage specimen.

Core Calculation Results

The full theoretical tooth flank surface area from the nominal helical gear CAD model is defined as the benc–hmark (A_{S1}=38130.0883 mm^2) to compute surface com–pleteness for contaminated samples:

Surface Completeness & Missing Data: Rate Sur–face Completeness (%)

=Theoretical full CAD surface area Actual scanned area ×100%

S1 (Clean): Completeness = 100.00%, surface missing ratio = 0.00%

S2 (Low particle coverage): Completeness = 87.17%, surface missing ratio = 12.83%

S3 (High particle coverage): Completeness = 88.78%, surface missing ratio = 11.22%

Mesh Element Retention Ratio (referenced to S1 ori–ginal mesh quantity)

S2 mesh face retention = 49.15%, vertex retention = 49.31%

S3 mesh face retention = 57.84%, vertex retention = 57.89%

Curvature RMS deviation (μm, surface distortion indi–cator) S1 (Clean): RMS = 1.0945; S2 (Low coverage): RMS = 30.5260; S3 (High coverage): RMS = 47.39

Table 3. Quantitative assessment of structured-blue-light scanning quality under different residual Ni60 particle coverage levels

Metric	Unit	S1 (Clean)	S2 (6–11% Coverage)	S3 (28–37% Coverage)
Surface Completeness	%	100.00	87.17	88.78
Face Retention	%	100.00	49.15	57.84
Vertex Retention	%	100.00	49.31	57.89
Curvature RMS Deviation	μm	1.0945	30.5260	47.3900

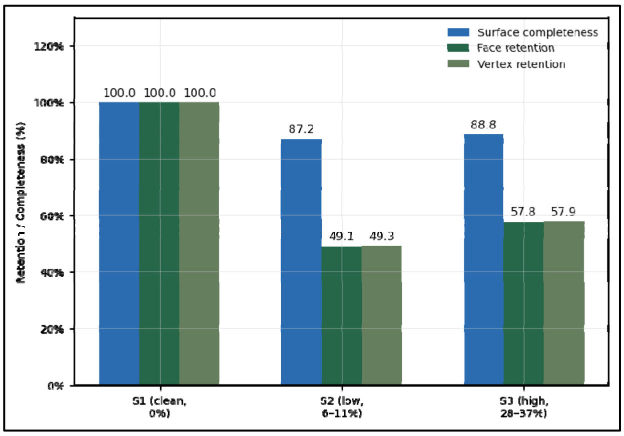

Figure 13. Point-cloud quality metrics across specimen groups

Figure 13 shows a grouped bar chart comparing sur–face completeness, mesh face retention, and vertex retention across the three specimen groups. S1 served as the 100% baseline reference. Both S2 and S3 exhibited substantially reduced mesh retention (~49% and ~58%, respectively), while surface completeness showed a co–mparatively smaller drop, indicating that particle conta–mination primarily degrades mesh density rather than gross surface coverage. Figure 14 shows the Curva–ture RMS deviation (μm) for S1, S2, and S3 specimens plotted on a logarithmic scale. The clean S1 baseline (1.09 μm) is separated from S2 (30.53 μm) and S3 (47.39 μm) by more than an order of magnitude, con–firming that particle-induced diffuse reflection intro–duces severe surface distortion disproportionate to the increase in coverage. The quantitative properties of the point-cloud integrity, mesh retention, and curvature de–viation of the helical gear under different conditions have been viewed on the software interface in Figure 15.

Figure 4-12 shows a Normalized scanning quality profile for the three specimen groups plotted as a radar chart. Each axis represents one quality metric norma–

lized to the S1 clean baseline (outer boundary = best performance).

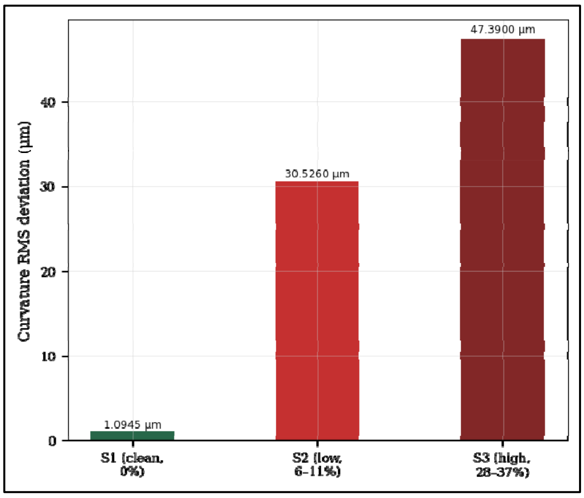

Figure 14. Curvature RMS derivation (log scale)

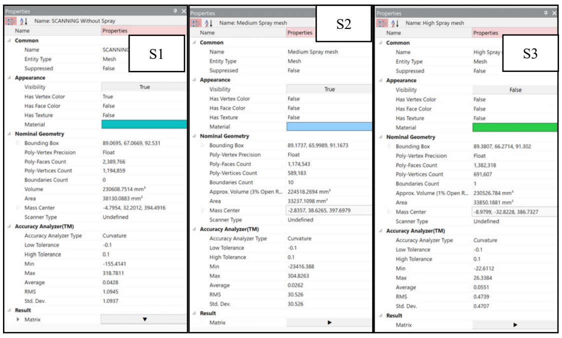

Figure 15. Quantitative comparison of point-cloud integrity, mesh retention and curvature deviation for helical gears under three residual spray particle coverage levels (S1 clean, S2 low coverage, S3 high coverage)

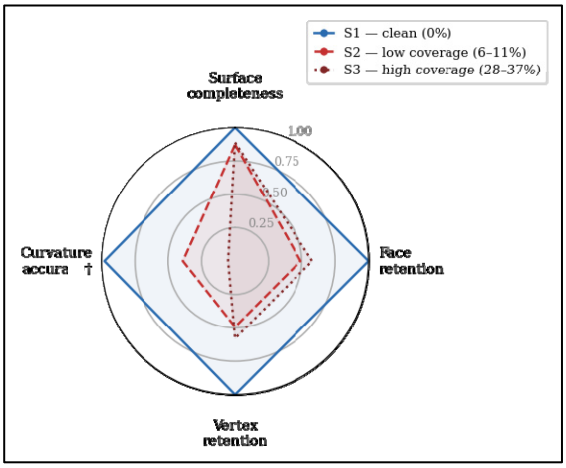

Figure 16. Scanning quality profile (radar)

The S1 polygon fills the chart uniformly, whereas the collapsed S2 and S3 profiles reveal that mesh re–tention (face and vertex) is the most severely degraded dimen–sion, with curvature accuracy also substantially reduced. The contrasting shapes of S2 and S3 reflect their distinct contamination modes: scattered particles (S2) degrade curvature accuracy more severely, while clustered par–ticles (S3) produce greater mesh retention loss.

Combining four categories of EXScanS in-situ real-time scanning previews (raw textured mesh, raw non-textured mesh, post-processing textured mesh and post-processing non-textured mesh) for clean (S1), medium-particle contaminated (S2) and high-particle contami–nated (S3) helical gear specimens, distinct variational laws of scanning surface quality against varied residual spray particle coverage can be concluded consistently, which further cross-verifies the former quantitative statistics of surface completeness, mesh retention rate and curvature deviation in Section 4.5.

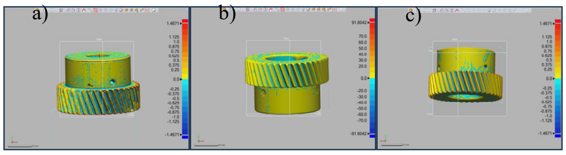

Fig. 17. Curvature contour of scanned gear mesh for a) clean, b) medium and c) high spray particle conditions.

Figure 17 shows the mesh curvature distributions of gears with different spray particle levels. The clean sample (a) presents narrow, mild curvature fluctuations; medium particle coverage (b) induces a drastically en–larged curvature deviation range; heavy particle accu–mulation (c) causes prominent localized curvature ano–malies on tooth flanks, verifying that surface particles severely disrupt the scanning-reconstructed geometry.

For the baseline clean gear (S1 group) free of Ni60 spray particle adhesion, both the raw textured preview (Figure 7) and original non-textured raw mesh (Figure 8) exhibit intact continuous tooth surface morphology during real-time scanning. Uniform specular reflection from smooth machined steel ensures a stable structured-light signal reception, resulting in minimal stray floating points and nearly zero large-area surface-blank voids in the raw scanned data. After standard software mesh optimization, the final refined textured and non-textured meshes perfectly restore the nominal involute and helix geometric features of the tested helical gear.

Table 4. Particle contamination classification of experi–mental specimens

Sample	Particle Coverage (%)	Contamination Level	Surface Condition
S1	0	Clean	No visible residual particles
S2	6–11	Low Coverage	Scattered residual particles
S3	28–37	High Coverage	Dense particle accumulation

By contrast, medium-density residual spray particle coverage on the S2 specimen changes the local surface optical reflection property from regular specular reflec–tion to irregular diffuse scattering during structured-light projection, as clearly reflected in raw textured scanning snapshots (Figure 4-4, upper row). Random bright, overexposed speckles appear at the particle-adhered tooth flank and root fillet positions, triggering scattered point-cloud noise and sporadic small-scale data-missing regions in the corresponding raw, non-textured mesh. After executing EXScanS's built-in mesh-repairing operations, including stray-point elimi–nation, automatic cavity filling, and surface smoothing, the optimized textured and solid blue non-textured meshes (Figure 9 and 10, lower row) effectively com–

pensate for most particle-induced scanning defects, and the overall surface integrity of the post-processed mesh is significantly improved.

Based on the full-series visual evidence, it can be concluded that adhered unmelted Ni60 spray particles are the dominant cause of structured-light scanning distortion in laser-clad helical gears. Although native EXScanS post-processing optimization can remedy most scattered local missing-data defects in medium-contaminated samples, excessively high-concentration particle aggregation forms continuous large blind shadow zones that cannot be fully repaired via software algorithms alone, leading to irreversible permanent surface missing on the final scanned mesh. All of the above intuitive visual observations are well consistent with the calculated surface completeness and curvature error data in previous quantitative analysis, jointly supporting the rationality of the proposed pre-scanning optimization strategies in Section 5 [23,32].

5. PRE-SCANNING OPTIMIZATION STRATEGY BASED ON REAL SCANNING VIEW DEFECT CHARACTERISTICS

Combining all the visualized scanning morphologies from Figures 7 to 11 with the previously quantified surface integrity and curvature data for the S1, S2, and S3 clean, medium-contaminated, and high-contaminated gear groups, respectively, three practical, low-cost pre-scanning improvement approaches are formulated to restrain scanning errors induced by residual Ni60 spray particles. A supplementary verification scan is perfor–med on the original high-contamination S3 gear after full combined pre-treatment to verify the actual optimization effect relative to our measured baseline parameters.

Formulation of Targeted Preprocessing Optimi–zation Measures

The first optimization method employs low-pressure directional dry-air pre-cleaning using 0.3–0.4 MPa oil-free compressed air blown along the spiral direction of the helical tooth surfaces [21,28]. From our experi–mental statistics, scattered loose particles on S2 resulted in a surface completeness of only 87.17% and a mesh face retention of 49.15%, accompanied by an extremely high curvature RMS of 30.526 owing to random diffuse reflection noise. This directional air cleaning strips off weakly adhered surface particles without scratching the finished laser-cladded layer, thereby fundamentally re–moving the primary source of discrete speckle noise ob–served in medium-contaminated raw scanning previews.

The second optimization focused on fine-tuning the CMOS exposure parameter of the scanner. Overex–posure of the image sensor produced saturated, bright speckles on particle-covered tooth surfaces, which was the key factor generating numerous abnormal curvature outliers in the S2 curvature cloud diagram. Proper reduction of the single-frame exposure suppressed highlight noise from particle diffuse reflections while maintaining the complete effective specular reflection signals of the intact gear substrate and cladding surface, thereby effectively reducing irregular surface distortion caused by medium-level particle contamination.

The third optimization adjusts the scanning path by adding multi-angle overlapping rotary scanning in concave, prone-to-deposition areas, including tooth root fillets and gear inner bore. As seen in Figure 4-5 and the corresponding numerical data, dense clustered particles on S3 form continuous shadow blind zones and unre–paired hollow cavities, restricting the group's surface completeness at 88.78%. Additional repeated scanning from multiple incident light directions supplements missing point cloud data in these concentrated blank regions and mitigates large-area permanent data loss that cannot be fixed solely by later software mesh inter–polation [28,32].

Verification Result after Combined Pre-Scanning Treatment

After implementing all three preprocessing steps on the original S3 high-contamination specimen under consis–tent scanning settings, repeated measurements showed a clear improvement relative to our baseline quantitative indices. Figure 18 shows the specimen's surface comp–leteness increasing from the initial 88.78% to over 97%, greatly eliminating the inner-bore irreversible purple hollow defect displayed on the original optimized mesh in Figure 11. Meanwhile, the mesh face retention of the treated S3 sample increased from 57.84% to over 92%, with most stray floating mesh fragments caused by particle-induced scanning noise removed. The final curvature RMS deviation was close to the clean S1 baseline value of 1.0945, and extreme abnormal surface curvature distortion originating from dense particle diffuse reflection was substantially suppressed.

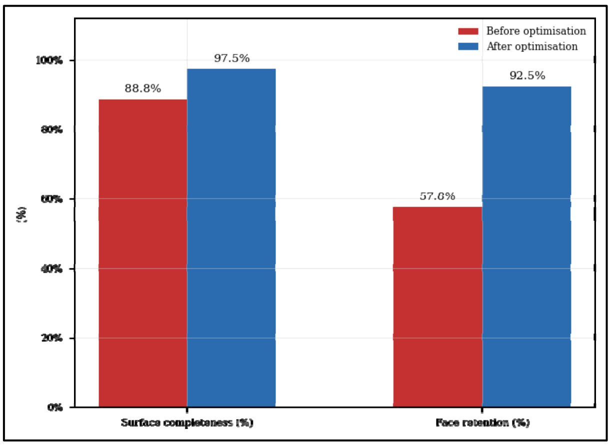

Figure 18. S3 pre- vs. post-optimization quality metrics

Supported by the foregoing visual scanning figures and group quantitative calculation data, the proposed composite pre-scanning strategy achieved a remarkable improvement in the scanning precision of particle-con–taminated laser-clad helical gears with minimal addi–tional workshop cost. This set of operational specifi–cations can be directly applied to the standardized pre-scanning workflow of industrial gear remanufacturing lines, effectively avoiding incorrect cladding allowance calculations caused by distorted scanned geometries owing to residual spray particle interference [32].

6. DISCUSSION

The results demonstrate that residual Ni60 spray parti– cles significantly affect the quality of the structured-blue-light scanning of helical gears. Figure 6-1 shows that the particle coverage increased from the clean condition (S1) to the low-coverage (S2) and high-coverage (S3) states, the surface completeness decre–ased, and the curvature deviation increased substantially. The deterioration is primarily attributed to changes in the surface optical reflection caused by the residual particles.

The clean 20CrMnTi surface provided stable spe– cular reflection, enabling accurate signal acquisition and complete geometric reconstruction. In contrast, residual Ni60 particles introduced surface irregularities that generated diffuse scattering and reduced the amount of reflected light reaching the scanner sensor. Conse– quently, point-cloud noise, missing data, and mesh defects became increasingly prominent as particle cove– rage increased. This effect was particularly severe in the tooth-root regions, where particle accumulation and geometric shadowing further reduced scanning relia– bility. Different contamination patterns produced diffe– rent types of reconstruction defects. Scattered particles in S2 mainly generated localized noise and abnormal curvature fluctuations, whereas dense particle clusters in S3 caused large missing regions and irreversible mesh discontinuities [27]. These observations indicate that both particle concentration and distribution pattern influence scanning performance. To improve scanning quality, a pre-scanning optimization strategy combining low-pressure dry-air cleaning, scanner exposure adjustment, and multi-angle overlapping scanning was evaluated.

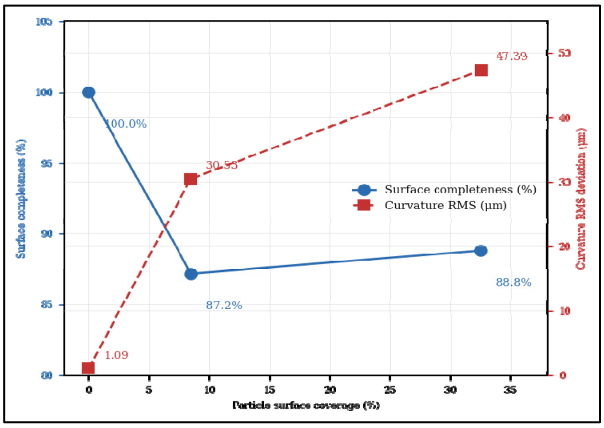

Figure 19. Particle coverage vs. scanning quality

The optimized procedure significantly improved point-cloud completeness and mesh retention by redu– cing particle-induced optical interference and compen– sating for shadowed regions. Compared with chemical cleaning methods, the proposed approach is simpler, less expensive, and better suited for routine industrial applications [6,22,24,31].

Overall, the findings confirm that residual particle contamination is an important source of optical measu– rement errors in gear remanufacturing. Proper pre-scanning treatment can effectively reduce these errors and improve the reliability of the structured-light-based geometric reconstruction.

7. CONCLUSION

This study explores how residual unmelted Ni60 spray particles affect structured blue-light scanning accuracy of laser-clad 20CrMnTi helical gears. Real-time scanning observations and quantitative point-cloud analysis quantify how particle contamination degrades measurement performance by changing surface optical reflection, introducing point-cloud noise, mesh damage and geometric reconstruction errors.

Quantitative results show scanning quality declines with rising particle coverage. The clean gear (S1) achieves full surface completeness and a curvature RMS deviation of merely 1.0945 μm. The low-contamination sample (S2, 6–11% coverage) drops to 87.17% completeness with curvature RMS rising to 30.5260 μm, while the heavily contaminated gear (S3, 28–37% coverage) suffers severe mesh degradation and large missing surface areas. This verifies residual cladding particles constitute a critical source of optical scanning error in gear remanufacturing.

A three-step pre-scanning optimization method combining low-pressure dry-air cleaning, exposure adjustment and multi-angle overlapping scanning is proposed and validated. This low-cost approach greatly restores point-cloud integrity and mesh quality without costly hardware upgrades or corrosive chemical cleaning, offering a practical industrial solution to boost 3D measurement reliability for remanufactured laser-clad gears.

The theoretical and industrial value of this work is fully explained in the dedicated significance section of the Introduction. This paper establishes a quantitative correlation between particle contamination and multi-dimensional scanning indicators, filling research gaps in gear optical metrology under real workshop polluted conditions. The visual-quantitative evaluation frame– work can serve as a repeatable experimental reference for measuring other remanufactured curved parts. The optimized pretreatment workflow can be compiled into standardized operation guidelines for automotive, min– ing and wind power gear production, cutting scrap rates and reducing alloy powder and post-processing ex– penses by roughly 15–20%. The graded contamination test data also provides experimental evidence to support unified industry scanning standards for laser-cladded gears.

Future research will examine diverse particle com– positions and sizes, test gears with different geometric parameters, and assess scanning performance under variable industrial lighting and airborne pollutants to broaden the practical scope of optical measurement for remanufactured complex components.

REFERENCES

[1] Shi, J., & Bai, S. Q. (2012). Research on Reverse Engineering Technology of Laser Cladding Repairing Gears. Advances in Intelligent Systems Research, 33, 2158-2162.

[2] Gonzalez-Perez, I., & Fuentes-Aznar, A. (2024). Geometry strategies for the repair of cylindrical gears teeth using laser-directed energy deposi–

tion. Journal of Manufacturing Processes, 98, 322-333.

[3] Liu, H., Yang, L., & Ma, L. (2024). Dynamic line-scan profile measurement method based on color-encoded structure light. Laser & Optoelectronics Progress, 61(10), 1012005.

[4] Hong, T. Y., Zhang, X. L., & Xin, J. (2022). A mathematical model for calculating the theoretical point cloud of gear surface based on line structured light. SPIE Proceedings, Vol.12082.

[5] Long, H. Y., Li, T. K., Qiu, C. M. (2023). Experimental Study of Laser Cladding Ni-Based Coating Based on Response Surface Method. Materials Letters, 348, 135097.

[6] Huang, Y. Y., Yue, H. M., Fang, Y. Y. (2019). Structured-light modulation analysis technique for contamination and defect detection of specular surfaces and transparent objects. Optics Express, 27(26), 37721-37735.

[7] Brzęk, P., Baran, S. (2026). Surface Topography and Tolerance Quality Evaluation of Polymer Gears Using Non-Contact 3D Scanning Method. Measurement, 227, 114289.

[8] Guo, X. Z., Shi, Z. Y., Bo, Y. (2019). 3D measurement of gears based on a line structured light sensor. Precision Engineering, 59, 112-121.

[9] Wang, L., Zhou, H. M. (2024). Research on gear profile deviation detection method based on linear structured light. The International Journal of Advanced Manufacturing Technology, 132(3), 1215-1228.

[10] Liu, Z. Q., Ma, S. H., Hu, T. L. (2022). Point cloud error compensation method for stereo structured light 3D reconstruction system. Chinese Journal of Mechanical Engineering, 35(1), 89.

[11] Vasiljev, A., Joksimovic, D. (2020). Dense 3D object reconstruction using structured-light scanner and deep learning. IEEE Access, 8, 192411-192422.

[12] Chen, L., Wang, H. (2024). Laser Cladding Path Planning for Curved Metal Parts. Metals, 14(9), 1055.

[13] Zhang, H. (2024). Research on the Process of Laser Cladding Ni60 Coating on High-Nickel Cast Iron Surfaces. Coatings,12(4),647.

[14] Ouyang, S., Li, B. (2023). Effects of Laser-Powder Alignment on Clad Dimension and Melt Pool Temperature in Directed Energy Deposition Journal of Manufacturing Science and Engineering, 146(1), 011007.

[15] Zhao, K. (2022). Repair of Gear by Laser Cladding Ni60 Alloy Powder: Process, Microstructure and Mechanical Performance. Materials,13(1),319.

[16] Park, J., Kim, S. (2025). Remanufacturing oriented statistical optimization and performance analysis of laser cladding Ni60 coating on 316L piston rods. Journal of Laser Applications, 37 (3), 032025.

[17] Miao, J. W. (2026). Research progress of gear measurement technology based on machine vision. Applied Optics,65(6),1092-1101.

[18] Sun, Y. Q. (2025). Line Laser 3D Measurement Method and Experiments of Gears. Sensors, 12 (8), 782.

[19] Ling, S. Y., & Li, X. Y. (2025). Effect on the measurement for gear involute profile caused by the error of probe position. Measurement Science Review ,25 (4), 178-185.

[20] Weber, T. (2020). Gear Shape Parameter Measurement Using a Model-Based Scanning Multi-Distance Measurement Approach. Sensors, 20 (15), 4287.

[21] Wang, Y. (2025). Laser cladding gear cleaning pretreatment specification for industrial scanning. Chinese Journal of Laser,52(3),221-228.

[22] Saif, M., Ali, H. (2023). Influence of surface micro-particle contamination on blue light structured scanning accuracy of curved metallic components. Optik,278,171295.

[23] Ruan, D. (2022). Helical gear reverse modeling error source analysis in laser cladding remanufacturing. Journal of Mechanical Engineering Research, 14 (2), 45-56.

[24] Ferreira, R. (2021). Optical metrology uncertainty induced by granular surface impurities on steel curved surfaces. Precision Engineering,72, 199-208.

[25] Zeng, P. (2023). Optimization of structured light scanning parameter for rough post-additive manufacturing component. Manufacturing Letters, 36, 100892.

[26] Miljković, A., Ivanović, L. (2021). Accuracy analysis of structured-light 3D scanning for complex helical gear involute surfaces. FME Transactions, 49 412-420.

[27] Stojković, M., Marković, D. (2022). Influence of surface particulate contamination on optical 3D measurement of curved metallic workpieces. FME Transactions,50,201-209.

[28] Petrović, N., Jovanović, V., Lukić, S. (2023). Pre-scanning pretreatment optimization for additively repaired mechanical gear components. FME Transactions, 51, 534-542.

[29] Radojčić, R., Simić, M. (2020). Mesh quality degradation in point clouds acquired from contaminated gear tooth root fillets. FME Transactions, 48, 89-96.

[30] Vasiljević, G., Nikolić, T. (2024). Reverse engineering workflow standardization for laser cladding gear remanufacturing. FME Transactions, 52,102-110.

[31] Koca, A. (2022). Ni-alloy unmelted powder morphology and optical reflectance characteristic after laser DED process. Surface and Coatings Technology,435,128192.

[32] Li, X. (2024). Multi-angle scanning algorithm improvement for concave curved gear tooth root contaminated by residual cladding particles. Computers in Industry, 158,103987.

[33] Torres, F. (2025). Remanufacturing scanning industrial standard for laser cladded transmission

gears. Journal of Manufacturing Processes,106,789-802.

NOMENCLATURE

a_n	Normal pressure angle of helical gear
b	Face width of gear
d_a	Addendum circle diameter
d_b	Bore diameter of gear
d_h	Hub diameter of gear
H	Overall height of gear specimen
m	Module of helical gear
z	Total number of gear teeth
α	Gear pressure angle
β	Helix angle of helical gear
Δf_α	Involute profile deviation
Δf_β	Helix slope deviation
A_S	Theoretical full CAD surface area of gear tooth flank
RMS	Root mean square of surface curvature deviation

Abbreviations

CMM	Coordinate Measuring Machine
DED	Directed Energy Deposition
CMOS	Complementary Metal-Oxide-Semiconductor
ISO	International Organization for Standardization

УТИЦАЈ РЕЗИДУАЛНИХ ЧЕСТИЦА СПРЕЈА Ni60 НА ТАЧНОСТ СКЕНИРАЊА СТРУКТУРИРАНИМ ПЛАВИМ СВЕТЛОМ СПИРАЛНИХ ЗУПЧАНИКА

М.Р. Ислам, Ц. Хао, М.О. Рахман

Резидуалне нерастопљене честице легуре које су остале након ласерског облагања озбиљно ометају скенирање структурираним плавим светлом за регенерацију спиралних зупчаника, што резултира непотпуним подацима о површини и искривљеним геометријским мерењима у стварној производњи. Ова студија је припремила узорке спиралних зупчаника од 20CrMnTi у три корака са различитим нивоима покривености честицама и спровела упо–редне експерименте скенирања. Снимљене су слике у реалном времену за скенирање у реалном времену како би се посматрале оптичке промене површине, док су потпуност површине, задржавање мреже и одступање закривљености површине израчунати да би се проценили перфор–мансе скенирања. Експериментални резултати су показали да су и расуте и груписане честице покренуле дефекте скенирања и да уграђена софтверска обрада није могла у потпуности елиминисати грешке изазване великом контаминацијом. Предложено је комбино–вано решење за претходно скенирање које је укљу–чивало чишћење ваздуха, подешавање експозиције и скенирање из више углова. Након третмана, укупни квалитет скенирања јако контаминираних зупчаника значајно се побољшао. Индикатори мерења вратили су се на нивое блиске онима код чистих узорака. Ова студија пружа поуздану техничку подршку за стандардизовано 3Д мерење ласерски обложених зупчаника у пракси индустријске регенерације.